THEORETICAL AND APPLIED MECHANICS
Volume 46 (2019) Issue 2, 173–189 DOI: https://doi.org/10.2298/TAM190801011S

A PAIRED QUASILINEARIZATION METHOD FOR SOLVING THE MHD MIXED CONVECTION FLOW OF A MICROPOLAR FLUID THROUGH A TRUNCATED CONE IN A NON-DARCY POROUS MEDIUM

Mekonnen Shiferaw Ayano, Sandile Sydney Motsa, and Olumuyiwa Otegbeye

Abstract. The aim of this paper is to investigate the flow, heat and mass transfer through a truncated cone in a non-Darcy porous medium in the presence of a transverse magnetic field by considering chemical reaction and radiation effects where the fluid is micropolar. The nonlinear equations governing the flow are solved using the paired quasilinearization method (PQLM). The study reveals that increasing radiation parameter, mixed convection parameter and Forchheimer number decreases microrotation. It is also noted that an increase in the radiation parameter leads to a corresponding increase in both the velocity and temperature of the fluid.

1. Introduction

Combined heat and mass transfer in fluid-saturated porous media are growing in importance in many manufacturing and environmental systems. These include heat exchanger devices, petroleum reservoirs, grain storage systems, heat pipes, chemical catalytic reactors, distillation towers, ion exchange columns, subterranean chemical waste migration, solar power absorbers, and others. A thorough discussion of these and other applications is available in the monographs of Ingham and Pop [1] and Nield and Bejan [2].

Most studies pertinent to porous media have been based on Darcy's law, which states that the volume-averaged velocity is proportional to the pressure gradient. In many practical applications, for example, packed sphere beds, the porous medium is bounded by an impermeable wall, has higher flow rates, and reveals nonhomogeneous porosity variation near the wall, making Darcy's law inapplicable [3]. Sheri and Shamshuddin [4] investigated the effects of diffusion-thermo, heat absorption and homogeneous chemical reaction on the free convective flow of a micropolar

2010 *Mathematics Subject Classification:* 76W05; 76U05; 65N35.
Key words and phrases: micropolar, non-Darcy, chemical reaction, magnetohydrodynamics(MHD), paired quasilinearization, spectral collocation.

fluid through a semi-infinite vertical plate. The important non-Darcian phenomenon of convective heat transport in porous media has generated lots of interest from various researchers. Inertial effects on porous media transport have been generally studied using the Darcy-Forchheimer model which uses a quadratic impedance term for inertial drag.

In literature, fluid flow about a full cone or frustum has been investigated quite extensively by [5–7, 9–11] amongst others. Recently Pullepu et al. [12] studied the unsteady laminar free convection from a vertical cone with uniform surface heat flux. In this numerical study, they observed that as the semi-vertical angle of the cone increases, velocity decreases. Gouse et al. [13] numerically studied an unsteady free convective heat and mass transfer in a Walters-B viscoelastic fluid flow along a vertical cone. In this study, it was reported that an increase in Schmidt number significantly decreased both velocity and concentration. More recently, free convection from a truncated cone subject to constant wall heat flux in a micropolar fluid was examined by Postelnicu [14]. In his analysis, he complemented an earlier study he conducted in [15] by obtaining results using the local non-similarity method. The effect of radiation on the mixed convection about a cone embedded in a porous medium filled with a nanofluid was studied by Chamkha et al. [16] and it included investigating the effects of Brownian motion and thermophoresis with Rosseland diffusion approximation.

Postelnicu [17] considered the development of the steady mixed convection boundary layer flow on a vertical impermeable frustum of a cone in a nanofluid. He reported the existence of dual solutions for the case of opposing flows. It is also reported in the study that the range of values of the mixed convection parameter for which solutions do exist increases in the presence of nanofluids.

Micropolar convection flows have been analyzed by many authors following the seminal work of Eringen [18] who introduced the micropolar fluid. A subclass of these fluids introduced by Eringen [19] is the micropolar fluid which exhibits the micro rotational effects observed in colloidal solutions, blood, dielectric fluids, plasmas, and liquid crystals amongst others. The monograph on the theory and applications of micropolar fluids has been reported by Ariman et al. [20, 21] and Lukaszewicz [22]. Micropolar fluids find applications in the purification of crude oil, polymer technologies, centrifugal separation processes, cooling tower dynamics, chemical reaction engineering, metallurgical drawing of filaments and solar energy systems.

To the best of our knowledge, no studies have been found in the literature on an MHD mixed convection micropolar fluid in a truncated cone within a porous medium with the simultaneous effects. In comparison to the Newtonian case, this model involves an extra equation in the governing equations and some additional parameters. This motivates the present study, where the main objective is to examine, numerically, the impact of key parameters such as the chemical reaction, radiation, mixed convection parameters and Forchheimer number with an efficient numerical method called the paired quasilinearization method (PQLM) [26, 27]. The convergence and accuracy of the PQLM are verified using solution error and residual error analysis, respectively. In the following sections, the physical model

and mathematical formulation of the problem are given. Subsequently, the implementation of the PQLM to obtain numerical solutions to the governing equations is performed and the results obtained are subsequently discussed in detail. Finally, the inference is made based on the observations.

2. Mathematical formulation of the problem

Consider the problem of the effect of a chemical reaction on a mixed convection boundary-layer flow of a magnetohydrodynamic (MHD) incompressible micropolar fluid near a vertical truncated cone as shown in Figure 1. Choose the Cartesian coordinate system with the origin 0 of the coordinate system placed at the vertex of the full cone. The x-axis is taken along the vertical frustum of a cone and y-axis is normal to the surface of the truncated cone. The truncated cone is either heated or cooled by convection from a fluid of temperature T_f with $T_f > T_\infty$ (heated surface) and $T_f < T_\infty$ (cooled surface), respectively. The solutal concentration is taken to be constant and is given by C_w. The velocity, far away from the truncated cone in the vertical direction, is U_∞, the temperature and concentration are T_∞ and C_∞, respectively. Under the above assumptions, along with the assumptions of Boussinesq and boundary layer approximations, the basic equations of a micropolar fluid governing the steady mixed convection boundary layer flow under the influence of a transversely applied magnetic field near a vertical frustum in a Darcy–Forchheimer saturated porous medium can be written as Postelnicu [17] and Chamkha [16]:

$$\frac{\partial(ur)}{\partial x} + \frac{\partial(vr)}{\partial y} = 0 \tag{2.1}$$

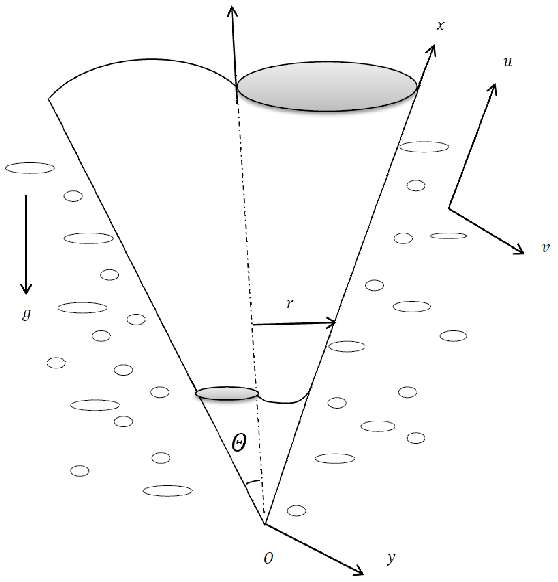

FIGURE 1. Geometry of the flow

$$u\frac{\partial u}{\partial x}+v\frac{\partial u}{\partial y}=\frac{\mu+\kappa}{\rho}\frac{\partial^2 u}{\partial y^2}+g^*[\beta_T(T-T_0)+\beta_c(C-C_0)]\cos\Theta + \kappa\frac{\partial \Gamma}{\partial y}-\sigma B_0^2 u-\frac{\nu}{K_p}u-\frac{b}{K_p}u^2 \tag{2.2}$$

$$\rho j\Big(u\frac{\partial \Gamma}{\partial x}+v\frac{\partial \Gamma}{\partial y}\Big)=\gamma\frac{\partial^2\Gamma}{\partial y^2}-2\kappa\Gamma-\kappa\frac{\partial u}{\partial y} \tag{2.3}$$

$$u\frac{\partial T}{\partial x}+v\frac{\partial T}{\partial y}=\alpha\frac{\partial^2 T}{\partial y^2}+\frac{\mu+\kappa}{\rho C_p}\Big(\frac{\partial u}{\partial y}\Big)^2+\frac{16\sigma^*}{3(a_r+\sigma_s)\rho C_p}\frac{\partial}{\partial y}\Big(T^3\frac{\partial T}{\partial y}\Big) \tag{2.4}$$

$$u\frac{\partial C}{\partial x}+v\frac{\partial C}{\partial y}=D\frac{\partial^2 C}{\partial y^2}-K_1(C-C_0) \tag{2.5}$$

where u and v are velocity components in the x and y directions, Γ is microrotation, ρ is the fluid density, μ, κ and γ are the material constants (viscosity coefficients), g^* is the acceleration due to gravity, K_p is the permeability of the porous medium, σ is the electrical conductivity of the fluid, β_T is the coefficient of thermal expansion, β_c is the coefficient of solutal expansion, B_0 is the magnetic field intensity, α is the thermal diffusivity, σ^*, a_r, σ_s are the Stefan-Boltzmann constant, scattering coefficient, and Rosseland mean extinction coefficient, respectively; r is the radius of the vertical frustum of a cone ($r = x\sin\Theta$), j is the micro-inertia density, C_p is the specific heat, D is the mass diffusivity and K_1 is the chemical reaction parameter.

The boundary conditions are given by

$$u=v=0,\quad \Gamma=-n\frac{\partial u}{\partial y},\quad -k\frac{\partial T}{\partial y}=h_f(T_f-T),\quad C=C_w,\qquad \text{at } y=0 \tag{2.6}$$

$$u=U_\infty,\quad \Gamma=0,\quad T=T_\infty,\quad C=C_\infty,\qquad \text{as } y\to\infty \tag{2.7}$$

where $n = 0$ gives the case where microelements close to the boundary stick to the wall and $n = 1$ corresponds to the turbulent boundary layer, k is the thermal conductivity of the fluid and h_f is the convective heat transfer coefficient.

Applying the following transformations

$$\begin{aligned}&\Psi=r\nu Re_x^{1/2}f(\zeta,\eta),\qquad \zeta=\frac{\bar{x}}{x_0}=\frac{x-x_0}{x_0},\qquad \eta=\frac{y}{\bar{x}}Re_x^{1/2}\\ &\Gamma=\frac{\nu Re_x^{3/2}}{\bar{x}^2}\omega(\zeta,\eta),\qquad \theta(\zeta,\eta)=\frac{T-T_\infty}{T_f-T_\infty},\qquad \phi(\zeta,\eta)=\frac{C-C_\infty}{C_w-C_\infty}\end{aligned} \tag{2.8}$$

where $Re_x=\frac{U_\infty\bar{x}}{\nu}$ is the local Reynolds number, Ψ is the stream function, which is defined as $u=\frac{1}{r}\frac{\partial\Psi}{\partial y}$ and $v=-\frac{1}{r}\frac{\partial\Psi}{\partial x}$. Substituting equation (2.8) into equations (2.1)–(2.5), we obtain the following non-dimensional equations

$$\frac{1}{1-N}f'''+\Big(\frac{\zeta}{1+\zeta}+\frac{1}{2}\Big)ff''+\Big(\frac{N}{1-N}\Big)\omega'+\zeta\lambda(\theta+\Delta\phi) -\zeta\frac{Ha^2}{Re_{xo}}f'-\zeta\frac{1}{D_aRe_{xo}}f'-\zeta\frac{F_s}{D_a}f'^2=\zeta\Big(f'\frac{\partial f'}{\partial\zeta}-f''\frac{\partial f}{\partial\zeta}\Big) \tag{2.9}$$

$$\frac{2-N}{2-2N}\omega'' + \Big(\frac{\zeta}{1+\zeta}+\frac{1}{2}\Big)f\omega' + \frac{1}{2}f'\omega - \zeta\Big(\frac{N}{1-N}\Big)(2\omega+f'') = \zeta\Big(f'\frac{\partial\omega}{\partial\zeta} - \omega'\frac{\partial f}{\partial\zeta}\Big) \tag{2.10}$$

$$\theta'' + Pr\Big(\frac{\zeta}{1+\zeta}+\frac{1}{2}\Big)f\theta' + Pr\delta\Big(\frac{1}{1-N}\Big)(f'')^2 + \frac{4}{3}RdRe_{xo}\zeta\{\theta'[(H-1)\theta+1]^3\}' = Pr\zeta\Big(f'\frac{\partial\theta}{\partial\zeta} - \theta'\frac{\partial f}{\partial\zeta}\Big) \tag{2.11}$$

$$\frac{1}{Sc}\phi'' + \Big(\frac{\zeta}{1+\zeta}+\frac{1}{2}\Big)f\phi' - K\phi = \zeta\Big(f'\frac{\partial\phi}{\partial\zeta} - \phi'\frac{\partial f}{\partial\zeta}\Big) \tag{2.12}$$

where the primes denote differentiation with respect to η, $\lambda = \frac{Gr_{x0}}{Re_{x0}^2}$ is the mixed convection parameter, $G_r = \frac{g*\beta_T(T_f-T_\infty)\bar{x}^3\cos\Theta}{\nu^2}$ is the thermal Grashof number, $G_c = \frac{g*\beta_c(C_w-C_\infty)\bar{x}^3\cos\Theta}{\nu^2}$ is the solutal Grashof number, $Rd = \frac{4\sigma^*T_\infty^3}{k(a_r+\sigma_s)}$ is the conduction radiation parameter, $H = \frac{T_w}{T_\infty}$ is the surface temperature excess ratio, $Ha = \frac{\sigma B_0^2 d^2}{\mu}$ is the Hartmann number, $D_a = \frac{K_p}{x_0^2}$ is the Darcy number, $F_s = \frac{b}{x_0}$ is the Forchheimer number, $\Delta = \frac{\beta_c(C_w-C_\infty)}{\beta_T(T_f-C_\infty)}$ is the buoyancy ratio, $N = \frac{\kappa}{\mu+\kappa}$ is the coupling number, $Pr = \frac{\nu}{\alpha}$ is the Prandtl number, $\delta = \frac{U_\infty^2}{C_p(T_f-T\infty)}$ is the viscous dissipation parameter, $Sc = \frac{\nu}{D_1}$ is the Schmidt number and $K = \frac{K_1x_o^2}{\nu}$ is the chemical reaction parameter.

The boundary conditions now take the form

$$f(\zeta,0) = -\frac{\zeta}{(\frac{\zeta}{\zeta+1}+\frac{1}{2})}\frac{\partial f}{\partial\zeta}, \qquad f'(\zeta,0)=0, \qquad \omega(\zeta,0) = -nf''(\zeta,0),$$
$$\theta'(\zeta,0) = -\zeta^{1/2}Bi(1-\theta(\zeta,0)), \qquad \phi(\zeta,0)=1, \qquad f'(\zeta,\infty)=1,$$
$$\omega(\zeta,\infty)=0, \qquad \theta(\zeta,\infty)=0, \qquad \phi(\zeta,\infty)=0 \qquad \text{as } \eta\to\infty$$

where $Bi = \frac{h_f x_o}{kRe_{xo}^{1/2}}$ is Biot number.

The non-dimensional skin friction, the Nusselt and Sherwood numbers are respectively given by

$$C_fRe_x^{1/2} = \Big(\frac{2}{1-N}\Big)f''(\zeta,0), \quad Nu_x = -Re_x^{1/2}\theta'(\zeta,0), \quad Sh_x = -Re_x^{1/2}\phi'(\zeta,0).$$

3. Numerical Scheme

To solve the nonlinear system of partial differential equations (2.9)–(2.12), the recently developed method of simplifying large systems, referred to as the paired quasilinearization method (PQLM) [26], is applied. The PQLM uses the ideas of the popular quasilinearization method (QLM) approach of Bellman and Kalaba [24] that seeks to simplify a system of equations through Taylor-series linearization before discretizing and solving using numerical methods. The essential difference

between the PQLM and the QLM is that the PQLM implements linearization on a pair of nonlinear functions within a pair of equations and uses updated solutions in subsequent pairs while the QLM linearizes a full system of equations at once. The problem under investigation in this study is well suited for the PQLM because of the nature of the boundary conditions for $f(\zeta,\eta)$ and $\omega(\zeta,\eta)$ which are coupled. This coupling suggests that $f(\zeta,\eta)$ and $\omega(\zeta,\eta)$ should be treated as a pair in the linearization process. Accordingly, an iteration scheme is developed on the assumption that when solving for f and ω at the current iteration, the values of the other unknowns θ and ϕ obtained from the previous iteration will be used. The iteration scheme is defined as

$$\Omega_1[F_{r+1}, W_{r+1}, T_r, P_r] = 0, \tag{3.1}$$

$$\Omega_2[F_{r+1}, W_{r+1}, T_r, P_r] = 0, \tag{3.2}$$

$$\Omega_3[F_{r+1}, W_{r+1}, T_{r+1}, P_r] = 0, \tag{3.3}$$

$$\Omega_4[F_{r+1}, W_{r+1}, T_{r+1}, P_{r+1}] = 0. \tag{3.4}$$

where $r+1$ and r denote the current and previous iteration, respectively, and Ω_1, Ω_2, Ω_3 and Ω_4 are nonlinear operators that denote equations (2.9), (2.10), (2.11) and (2.12), respectively, and F, W, T, P are defined as

$$F = \Big\{f, \frac{\partial f}{\partial \eta}, \frac{\partial^2 f}{\partial \eta^2}, \frac{\partial^3 f}{\partial \eta^3}, \frac{\partial f}{\partial \zeta}, \frac{\partial^2 f}{\partial \zeta \partial \eta}\Big\},$$

$$W = \Big\{\omega, \frac{\partial \omega}{\partial \eta}, \frac{\partial^2 \omega}{\partial \eta^2}, \frac{\partial \omega}{\partial \zeta}\Big\},$$

$$T = \Big\{\theta, \frac{\partial \theta}{\partial \eta}, \frac{\partial^2 \theta}{\partial \eta^2}, \frac{\partial \theta}{\partial \zeta}\Big\},$$

$$H = \Big\{\phi, \frac{\partial \phi}{\partial \eta}, \frac{\partial^2 \phi}{\partial \eta^2}, \frac{\partial \phi}{\partial \zeta}\Big\}.$$

We remark that, at the iteration level $r+1$, once equations (3.1) and (3.2) have been solved simultaneously for the unknowns F_{r+1} and W_{r+1}, equations (3.3) and (3.4) only have the unknowns T_{r+1} and P_{r+1}, respectively.

The linearization of the equations is applied using Taylor series expansion of Ω_k about some previous approximation of the solutions denoted by F_r, T_r, H_r, W_r. The assumption used is that the difference between the current and previous solution is small. The linearization process gives,

$$\frac{1}{1-N} f'''_{r+1} + [a_1] f''_{r+1} + [a_2] f'_{r+1} + [a_3] f_{r+1} + \Big(\frac{N}{1-N}\Big)\omega'_{r+1} = [a_4]\frac{\partial f'_{r+1}}{\partial \zeta} + [a_5]\frac{\partial f_{r+1}}{\partial \zeta} + a_6, \tag{3.5}$$

$$\Big(-\zeta\Big(\frac{N}{1-N}\Big)\Big) f''_{r+1} + [b_1] f'_{r+1} + [b_2] f_{r+1} + \Big(\frac{2-N}{2-2N}\Big)\omega''_{r+1} + [b_3]\omega'_{r+1} + [b_4]\omega_{r+1} = [b_5]\frac{\partial f_{r+1}}{\partial \zeta} + [b_6]\frac{\partial \omega_{r+1}}{\partial \zeta} + b_7, \tag{3.6}$$

$$[c_1]\theta''_{r+1} + [c_2]\theta'_{r+1} + [c_3]\theta_{r+1} = [c_4]\frac{\partial\theta_{r+1}}{\partial\zeta} + c_5, \tag{3.7}$$

$$\frac{1}{Sc}\phi''_{r+1} + [e_1]\phi'_{r+1} + (-K)\phi_{r+1} = [e_2]\frac{\partial\phi_{r+1}}{\partial\zeta}, \tag{3.8}$$

where

$$\begin{aligned}
&\alpha_1 = \frac{\zeta}{1+\zeta} + \frac{1}{2}, \quad \alpha_2 = \frac{1}{DaRe_{x_0}}, \quad \alpha_3 = \frac{4}{3Pr}Re_{x_0},\\
&\alpha_5 = \tfrac{4}{3}Re_{x_0}Rd, \quad Z = H - 1,\\
&a_1 = \alpha_1 f_r + \zeta\frac{\partial f_r}{\partial\zeta}, \quad a_2 = -\zeta\frac{Ha^2}{Re_{x_0}} - \zeta\alpha_2 - 2\zeta\frac{Fs}{Da}f'_r - \zeta\frac{\partial f'_r}{\partial\zeta},\\
&a_3 = \alpha_1 f''_r, \quad a_4 = \zeta f'_r, \quad a_5 = -\zeta f''_r,\\
&a_6 = \alpha_1 f_r f''_r - \zeta\lambda(\theta_r + \Delta\phi_r) - \zeta\frac{Fs}{Da}f'^2_r - \zeta f'_r\frac{\partial f'_r}{\partial\zeta} + \zeta f_r{}''\frac{\partial f_r}{\partial\zeta},\\
&b_1 = \frac{1}{2}\omega_r - \zeta\frac{\partial\omega_r}{\partial\zeta}, \quad b_2 = \alpha_1\omega'_r, \quad b_3 = \alpha_1 f_r + \zeta\frac{\partial f_r}{\partial\zeta}\\
&b_4 = \frac{1}{2}f'_r - 2\zeta\Big(\frac{N}{1-N}\Big), \quad b_5 = -\zeta\omega'_r, \quad b_6 = \zeta f'_r,\\
&b_7 = \alpha_1 f_r\omega'_r + \frac{1}{2}f'_r\omega_r - \zeta f'_r\frac{\partial\omega_r}{\partial\zeta} + \zeta\omega'_r\frac{\partial f_r}{\partial\zeta},\\
&c_1 = \frac{1}{Pr} + \alpha_3\zeta(1 + 3Z\theta_r + 3Z^2\theta_r^2 + Z^3\theta_r^3),\\
&c_2 = \alpha_1 f_{r+1} + \alpha_3\zeta(6Z\theta'_r + 12Z^2\theta_r\theta'_r + 6Z^3\theta_r^2\theta'_r) + \zeta\frac{\partial f_{r+1}}{\partial\zeta},\\
&c_3 = \alpha_3\zeta(6Z^2\theta'^2_r + 6Z^3\theta_r\theta'^2_r + 3Z\theta''_r + 6Z^2\theta''_r\theta_r + 3Z^3\theta''_r\theta_r^2),\\
&c_4 = \zeta f'_{r+1}, \quad e_1 = \alpha_1 f_{r+1} + \zeta\frac{\partial f_{r+1}}{\partial\zeta}, \quad e_2 = \zeta f'_{r+1},\\
&c_5 = \Big(\frac{-Pr\delta}{1-N}\Big)f''^2_{r+1} + 3\alpha_3\zeta(Z\theta'^2_r + 4Z^2\theta_r\theta'^2_r + 3Z^3\theta_r^2\theta'^2_r\\
&\qquad\qquad + Z\theta_r\theta''_r + 2Z^2\theta''_r\theta_r^2 + Z^3\theta''_r\theta_r^3),\\
&R_1 = a_6, \quad R_2 = b_7, \quad R_3 = c_5, \quad R_4 = 0.
\end{aligned}$$

The resulting decoupled system of linear pairs (3.5) – (3.8) can be solved using various numerical methods. In this study, the bivariate spectral collocation method with Chebyshev–Gauss–Lobatto nodes is employed. The discretization with spectral collocation is applied to both the space η and time ξ domains after transforming the original domains to $[-1,1]\times[-1,1]$. Linear transformations are used to transform the physical domains $\eta\in[0,\eta_\infty]$ and $\zeta\in[0,\zeta_\infty)$ to $\xi\in[-1,1]$ and $\tau\in[-1,1]$, respectively. Here, η_∞ and ζ_∞ are finite values chosen to be large enough to approximate the behaviour of the flow quantities at near infinity. These values are introduced to facilitate the application of the numerical method at infinity. The

discretization nodes are defined as

$$\xi_i = \cos\left(\frac{\pi i}{N_x}\right), \quad \tau_j = \cos\left(\frac{\pi j}{N_\tau}\right), \qquad i = 0, 1, \ldots, N_x; \quad j = 0, 1, \ldots, N_\tau.$$

The approximate solutions are assumed to be defined in terms of bivariate Lagrange interpolation polynomial of the form

$$f(\eta, \zeta) \approx \sum_{m=0}^{N_x} \sum_{j=0}^{N_\tau} f(\xi_m, \tau_j) L_m(\xi) L_j(\tau),$$

which interpolates $f(\eta, \zeta)$ at the Gauss-Lobatto collocation points. Similar expressions are used to define approximate functions for $\theta(\eta, \xi)$, $\phi(\eta, \xi)$ and $\omega(\eta, \xi)$.

The Chebyshev pseudo-spectral method is applied to (3.5)–(3.8) with derivatives of the unknown functions with respect to η and ζ at the collocation points ξ_k and τ_i defined as:

$$\left.\frac{\partial^n f}{\partial \eta}\right|_{(\xi_k, \tau_i)} = \mathbf{D}^n \mathbf{F}_i, \quad n = 1, 2, 3$$

$$\left.\frac{\partial f}{\partial \xi}\right|_{(\xi_k, \tau_i)} = \sum_{j=0}^{N_\tau} \mathbf{d}_{ij} \mathbf{F}_j,$$

where $\mathbf{d}_{i,j} = (2/\zeta_e) d_{i,j}$ $(i, j = 0, 1, \ldots, N_t)$ with $d_{i,j}$ being entries of the standard Chebyshev differentiation matrix $d = [d_{i,j}]$ of size $(N_\tau + 1) \times (N_\tau + 1)$ (see, for example Trefethen [25]). Similarly, $\mathbf{D} = (2/\eta_e)[D_{r,s}]$ $(r, s = 0, 1, 2, \ldots, N_x)$ with $[D_{r,s}]$ being an $(N_x + 1) \times (N_x + 1)$ Chebyshev derivative matrix, and the vector $\mathbf{F}_i$ is defined as

$$\mathbf{F}_i = [f_i(\xi_0), f_i(\xi_1), \ldots, f_i(\xi_{N_x})]^T.$$

Similar definitions are obtained for the partial derivatives of the other unknown functions.

The discretized forms of equations (3.5) − (3.8) are

$$\mathbf{A}^{(i)}_{1,1} \mathbf{F}_{r+1,i} + \mathbf{A}^{(i)}_{1,2} \mathbf{W}_{r+1,i} + \mathbf{a}_5 \sum_{j=0}^{N_\tau} \mathbf{d}_{i,j} \mathbf{F}_{r+1,j} + \mathbf{a}_4 \sum_{j=0}^{N_\tau} \mathbf{d}_{i,j} \mathbf{D}\mathbf{F}_{r+1,j} = \mathbf{R}_{1,i},$$

$$\mathbf{A}^{(i)}_{2,1} \mathbf{F}_{r+1,i} + \mathbf{A}^{(i)}_{2,2} \mathbf{W}_{r+1,i} + \mathbf{b}_5 \sum_{j=0}^{N_\tau} \mathbf{d}_{i,j} \mathbf{F}_{r+1,j} + \mathbf{b}_6 \sum_{j=0}^{N_\tau} \mathbf{d}_{i,j} \mathbf{W}_{r+1,j} = \mathbf{R}_{2,i},$$

$$\mathbf{A}^{(i)}_{3,3} \mathbf{\Theta}_{r+1,i} + \mathbf{c}_4 \sum_{j=0}^{N_\tau} \mathbf{d}_{i,j} \mathbf{\Theta}_{r+1,j} = \mathbf{R}_{3,i},$$

$$\mathbf{A}^{(i)}_{4,4} \mathbf{\Phi}_{r+1,i} + \mathbf{e}_2 \sum_{j=0}^{N_\tau} \mathbf{d}_{i,j} \mathbf{\Phi}_{r+1,j} = \mathbf{R}_{4,i},$$

for $i = 0, 1, 2, \ldots, N_\tau$ where the matrix coefficients and right hand side vectors are defined as

$$A^{(i)}_{1,1} = \frac{1}{1 - N} \mathbf{D}^3 + [\mathbf{a}_1]\mathbf{D}^2 + [\mathbf{a}_2]\mathbf{D} + [\mathbf{a}_3] - [\mathbf{a}_4]\mathbf{D}\mathbf{d}_{i,i}, \quad A^{(i)}_{1,2} = \frac{N}{1 - N} \mathbf{D},$$

$$A_{2,1}^{(i)} = \Big(-\zeta\Big(\frac{N}{1-N}\Big)\Big)\mathbf{D}^2 + [\mathbf{b}_1]\mathbf{D} + [\mathbf{b}_2] - [\mathbf{b}_5]\mathbf{d}_{i,i},$$
$$A_{2,2}^{(i)} = \Big(\frac{2-N}{2-2N}\Big)\mathbf{D}^2 + [\mathbf{b}_3]\mathbf{D} + [\mathbf{b}_4] - [\mathbf{b}_6]\mathbf{d}_{i,i},$$
$$A_{3,3}^{(i)} = [\mathbf{c}_1]\mathbf{D}^2 + [\mathbf{c}_2]\mathbf{D} + [\mathbf{c}_3] - [\mathbf{c}_4]\mathbf{d}_{i,i}\mathbf{a}_{1,2}^{(1)},$$
$$A_{4,4}^{(i)} = \frac{1}{Sc}\mathbf{D}^2 + [\mathbf{e}_1]\mathbf{D} + (-K)\mathbf{I} - [\mathbf{e}_2]\mathbf{d}_{i,i},$$

where $\mathbf{I}$ is an identity matrix of size $(N_x+1)\times(N_x+1)$.

4. Results and discussion

In this section, we present some numerical results obtained for the system of partial differential equations using the PQLM. We also investigate the influence of mixed convection, conduction radiation, chemical reaction and local Forchheimer parameter on the respective velocity, temperature, concentration and nano-particle concentration profiles. To generate these results, we used 50 grid-points in space and 20 grid-points in time as these were found to be adequate in generating solutions consistent to 9 decimal places. We begin by verifying the convergence, speed of convergence and accuracy of the PQLM. To display accuracy and convergence, we set $n = 0.1$, $N = 0.6$, $\Delta = 0.4$, $Ha = 1$, $Da = 10$, $Re = 1$, $Pr = 0.72$, $\delta = 0.2$, $H = 1$, $Fs = 1$, $Rd = 0.5$, $Sc = 0.22$, $K = 0.3$ and $Bi = 10$.

To further investigate the convergence of our numerical scheme, the solution error norm is calculated. This is done by obtaining the infinity norm of the difference between solutions obtained with successive iterations. If the error between the solutions gets smaller until a point where a further increase in iterations does not change the error, the method converges. Figures 2a to 2b display the solution error norms for $\mathbf{F}$, $\mathbf{\Omega}$, $\mathbf{\Theta}$ and $\mathbf{\Phi}$. We observe from Figures 2a and 2b that as the number of iterations increase, the error keeps getting smaller until the 35^{th} iteration when it converges to a solution error of 10^{-60}. Thereafter, we observe that a further iteration does not impact on the error. This indicates that the PQLM converges. It

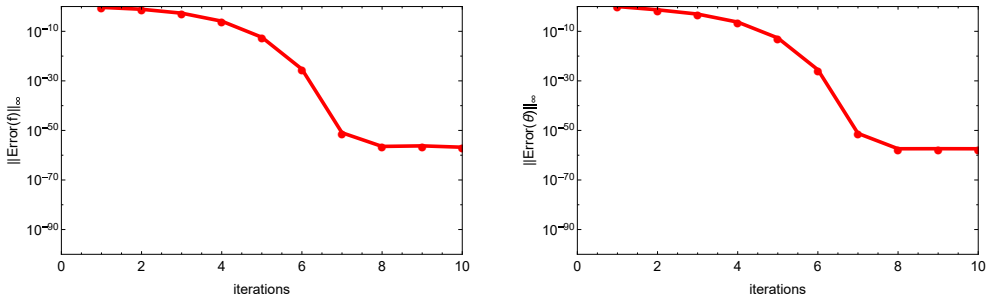

(a) Solution error norm of $\mathbf{F}$ (b) Solution error norm of $\mathbf{\Theta}$

FIGURE 2. Effect of iterations on the solution error norms when $\xi = 0.4$

is also observed from the slopes of the respective figures that the PQLM converges quadratically and hence quickly.

To verify the accuracy of the PQLM, we calculate the residual error by substituting the original system of equations with the approximate solutions obtained. This shows us the proximity of our solutions to the exact solutions to the system of differential equations.

Figures 3a to 3b display the effect of iterations on the residual error norms of equations (2.9)–(2.12).

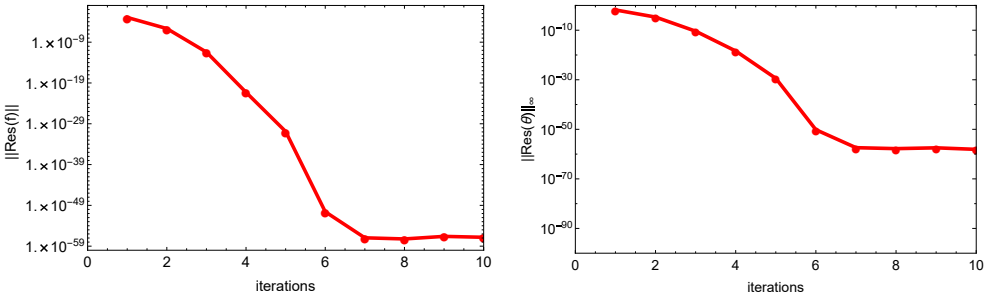

(a) Residual error norm of $\mathbf{F}$ (b) Residual error norm of $\mathbf{\Theta}$

FIGURE 3. Effect of iterations on the residual error norms when $\zeta = 0.8$

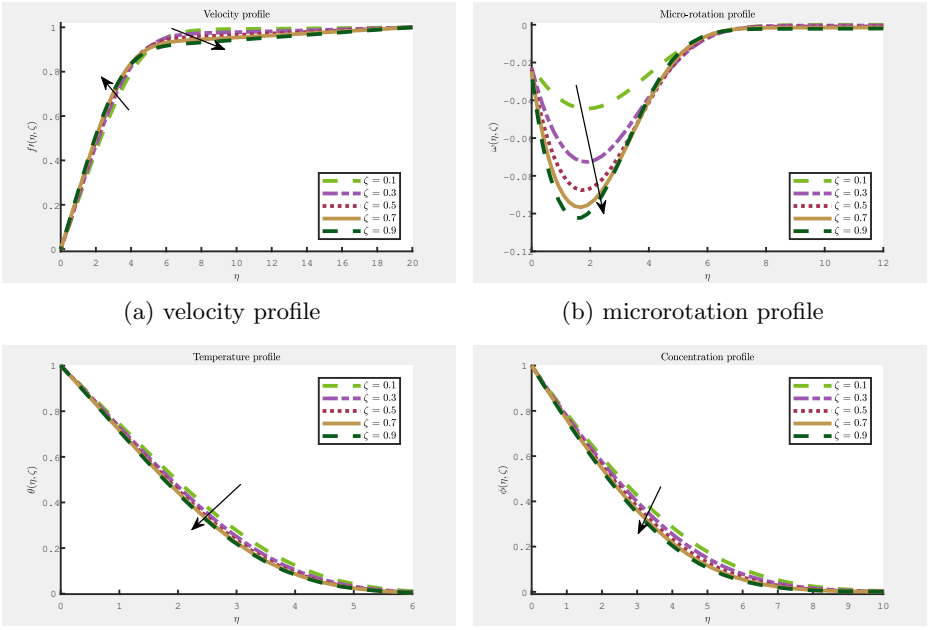

(a) velocity profile (b) microrotation profile

(c) temperature profile (d) concentration profile

FIGURE 4. Effect of time ζ on the flow profiles

From Figures 3a and 3b, it is observed that as the system is being iterated, the residual error improves until the 7^{th} iteration when the error is 10^{-58}. This represents a very small number and hence indicates that the PQLM is a highly accurate method for solving similar problems.

TABLE 1. Effect of mixed convection, Hartmann number, conduction radiation and Forchheimer number on the skin friction, Nusselt number and Sherwood number

K	Ha	Rd	Fs	$\frac{2}{1-N}f''(\xi,0)$	$\frac{2}{1-N}\omega'(\xi,0)$	$-Re_x^{1/2}\theta'(\eta,0)$	$-Re_x^{1/2}\phi'(\eta,0)$
0	0.2	0.1	1	0.423174	-0.217633	-0.074370	-0.233213
0.5	0.2	0.1	1	0.420141	-0.216072	-0.074370	-0.389500
1	0.2	0.1	1	0.418374	-0.215164	-0.074370	-0.505174
2	0.2	0.1	1	0.416216	-0.214054	-0.074369	-0.684176
0.1	0	0.1	1	2.477194	1.301483	0.052504	0.200644
0.1	0.1	0.1	1	2.383719	1.243044	0.052537	0.198243
0.1	0.2	0.1	1	2.111914	1.077212	0.052588	0.190891
0.1	0.3	0.1	1	1.689826	0.832990	0.052505	0.178118
0.1	0.2	1	1	2.119285	1.082616	0.052424	0.191096
0.1	0.2	3	1	2.137405	1.096239	0.051610	0.191542
0.1	0.2	5	1	2.154632	1.109190	0.050730	0.191944
0.1	0.2	7	1	2.170410	1.120998	0.049906	0.192305
0.1	0.2	0.1	0	0.257967	-0.132669	-0.073751	-0.231595
0.1	0.2	0.1	0.1	0.237818	-0.122307	-0.073534	-0.225319
0.1	0.2	0.1	0.3	0.223246	-0.114812	-0.073341	-0.220543
0.1	0.2	0.1	0.4	0.192185	-0.098838	-0.072798	-0.209558

Table 1 displays the effect of mixed convection, Hartmann number, conduction radiation and Forchheimer number on the skin friction, Nusselt number and Sherwood number. The set parameter values are $Re = 0.5$, $n = 0.8$, $\lambda = 0.2$, $\Delta = 0.1$, $Da = 10$, $Pr = 0.72$, $\delta = 0.1$, $H = 1.2$, $Sc = 0.22$, $Z = H - 1$ and $N = 0.6$. As displayed in Table 1, it can be seen that as mixed convection increases, skin friction decreases while the Sherwood number increases. There appears to be no visible effect on the Nusselt number. When the Hartmann number is increased, the skin friction and Sherwood number both decrease while the Nusselt number increases. An increase in radiation however increases the skin friction and Sherwood number while decreasing the Nusselt number. The skin friction, Nusselt number and Sherwood number all decrease with an increase in the Forchheimer number.

Given that the flow is governed by various parameters, this study focuses on the influence of select parameters such as time (ζ), mixed convection (λ), conduction radiation (Rd), chemical reaction (K) and local Forchheimer parameter (Fs) on the velocity, microrotation, temperature and concentration flow profiles, and unless varied, we set $Re = 10$, $Rd = 0.5$, $n = 0.8$, $N = 0.6$, $\Delta = 0.1$, $Ha = 0.2$, $Da = 10$, $Fs = 1$, $Pr = 0.72$, $\delta = 1$, $\lambda = 0.1$, $H = 1.2$, $Sc = 0.22$, $K = 0.1$, and $Bi = 10$.

Figures 4a to 4d display the effect of time ζ on the velocity, microrotation, temperature and concentration profiles.

We observe from Figure 4a that for $0 \leqslant \eta \leqslant 5$, the velocity profile increases as time increases but decreases when $\eta > 5$. In Figure 4b, however, the microrotation profile is seen to decrease as ζ increases. We also observe from Figures 4c and 4d that an increase in ζ decreases the temperature and concentration profiles, respectively.

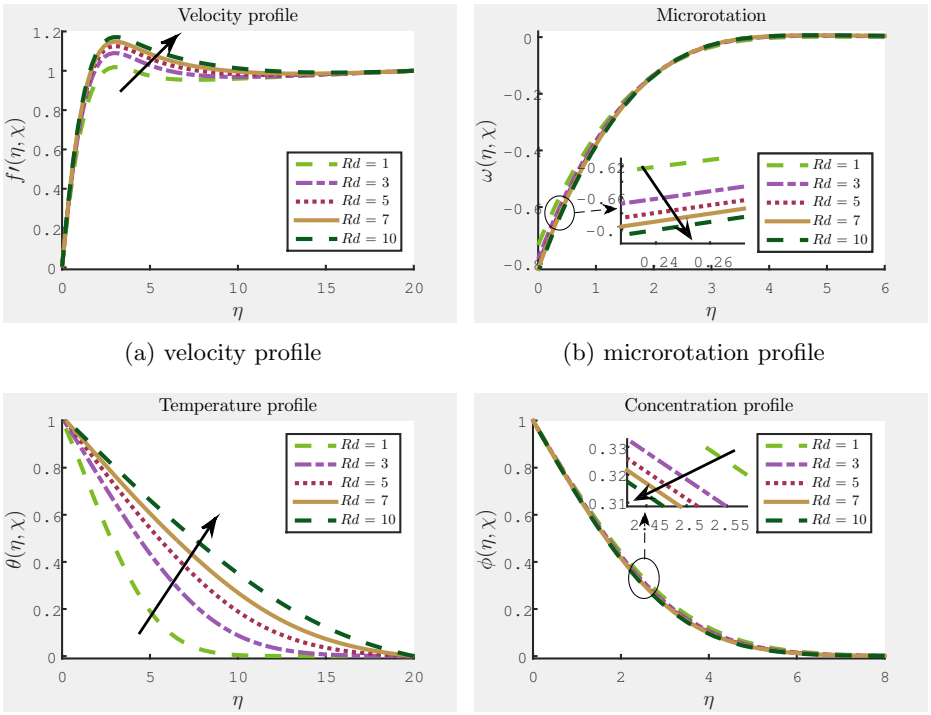

(a) velocity profile

(b) microrotation profile

(c) temperature profile

(d) concentration profile

FIGURE 5. Effect of radiation Rd on the flow profiles

Figures 5a to 5d show the effect of varying the amount of radiation on the flow profiles. An increase in radiation is observed to heat the fluid and thereby facilitate the upward flow of the fluid in the cone thus reducing the microrotation. This is seen in Figures 5a and 5b where the velocity flow increases while the microrotation decreases. With an increase in radiation on the fluid, the fluid heats up thereby increasing temperature within the cone and decreasing concentration of the fluid as diffusion occurs. We can see these trends in Figures 5c and 5d.

Figures 6a to 6d display the effect of the local Forchheimer parameter on the velocity, microrotation, temperature and concentration profiles.

We observe that the velocity profile decreases as Fs increases with a less significant effect near the boundary layer as seen in Figure 6a. In Figure 6b, we can see that for $0 \leqslant \eta \leqslant 2$, Fs increases the microrotation profile and decreases the

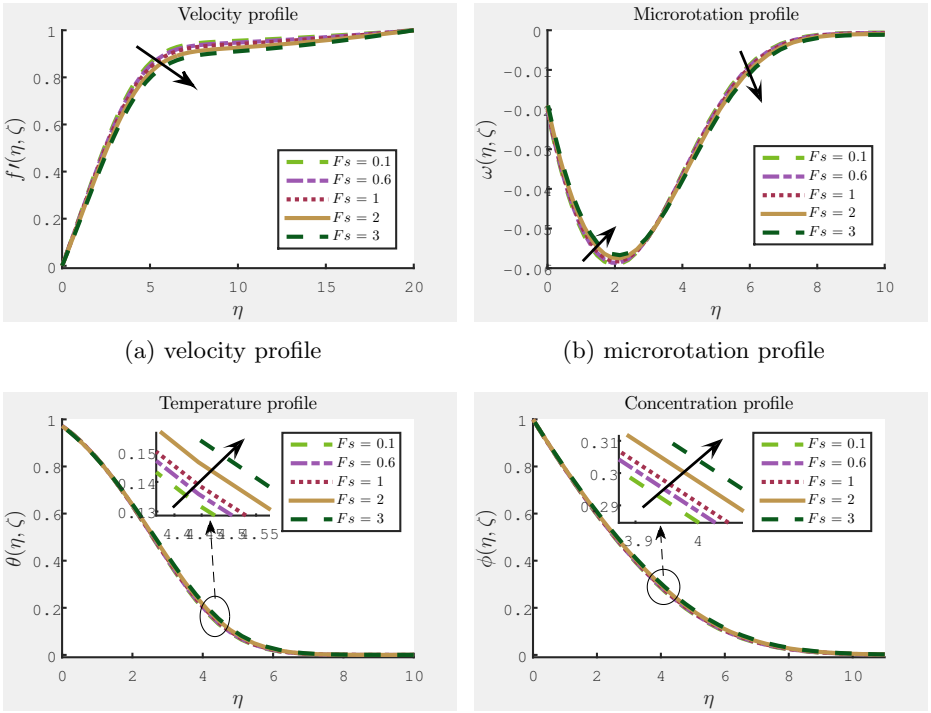

(a) velocity profile (b) microrotation profile

(c) temperature profile (d) concentration profile

FIGURE 6. Effect of local Forchheimer parameter Fs on the flow profiles

profile for $\eta > 2$ showing a rotational effect. The concentration and temperature profiles are observed to increase as Fs increases in Figures 6c and 6d.

Figures 7a to 7d display the effect of an increasing chemical reaction on the various flow profiles. While an increase in K decreases the velocity profile, the microrotation profile is observed to increase. An increasing chemical reaction in the cone will effectively heat up the fluid faster and this reaction will decrease the concentration of the fluid. This expected trend is observed in Figures 7c and 7d where we observe an increment in the temperature profile and decrease in the concentration profile as K is increased.

Figures 8a to 8d show the influence of mixed convection on various profiles. We observe that as λ increases, the velocity flow profile increases while the microrotation profile decreases in Figures 8a and 8b, respectively. We also observe that temperature and concentration both decrease with an increase in λ.

5. Conclusion

In this study, we have observed the influence of conduction radiation, mixed convection, chemical reaction and Forchheimer parameter on the boundary layer flow of an MHD incompressible micropolar fluid near a vertical truncated cone. The

study has been conducted using the recently introduced paired quasi-linearization method (PQLM) to generate required results. From the results obtained, it has been observed that:

- Microrotation decreases as radiation, mixed convection and Forchheimer number increase,
- An increase in the size of the frustum leads to a corresponding decrease of the velocity, microrotation, temperature and concentration profiles,
- Microrotation shows an increase in its reverse flow for $0 \leqslant \eta \leqslant 5$ as time increases,
- Increasing the mixed convection parameter increases the velocity profile while decreasing the microrotation, temperature and concentration profiles.
- An increase in the Forchheimer parameter decreases the velocity of the fluid flow and the microrotation far from the boundary layer.
- Skin friction, Nusselt number and Sherwood number decrease in magnitude with an increase in both the Forchheimer and Hartmann number.
- The radiation parameter increases the velocity of the fluid and the temperature while decreasing the microrotation and concentration.

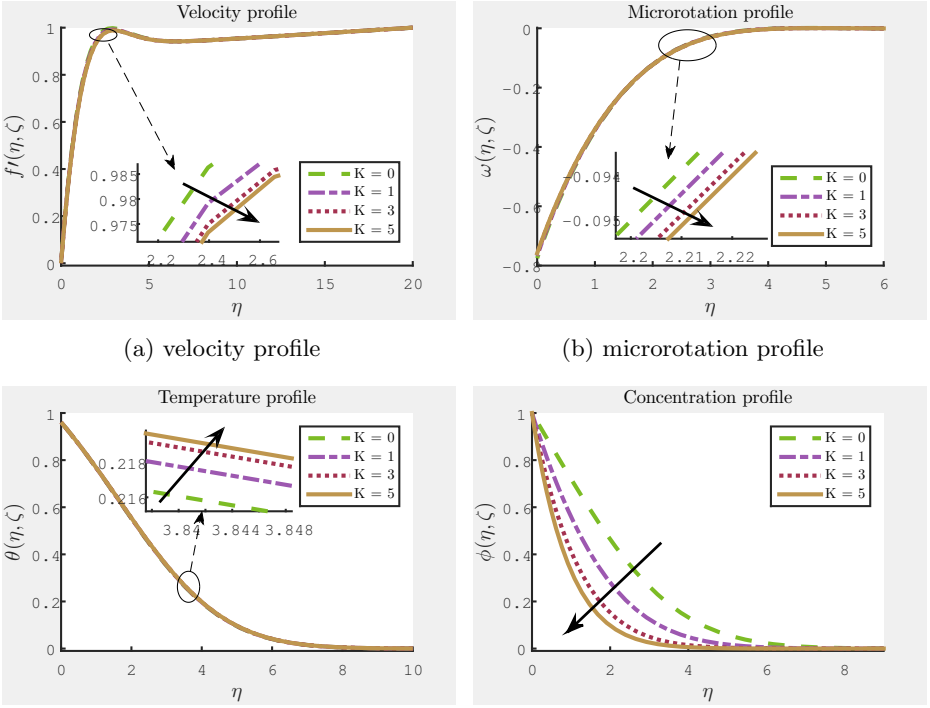

(a) velocity profile (b) microrotation profile

(c) temperature profile (d) concentration profile

FIGURE 7. Effect of chemical reaction K on the flow profiles

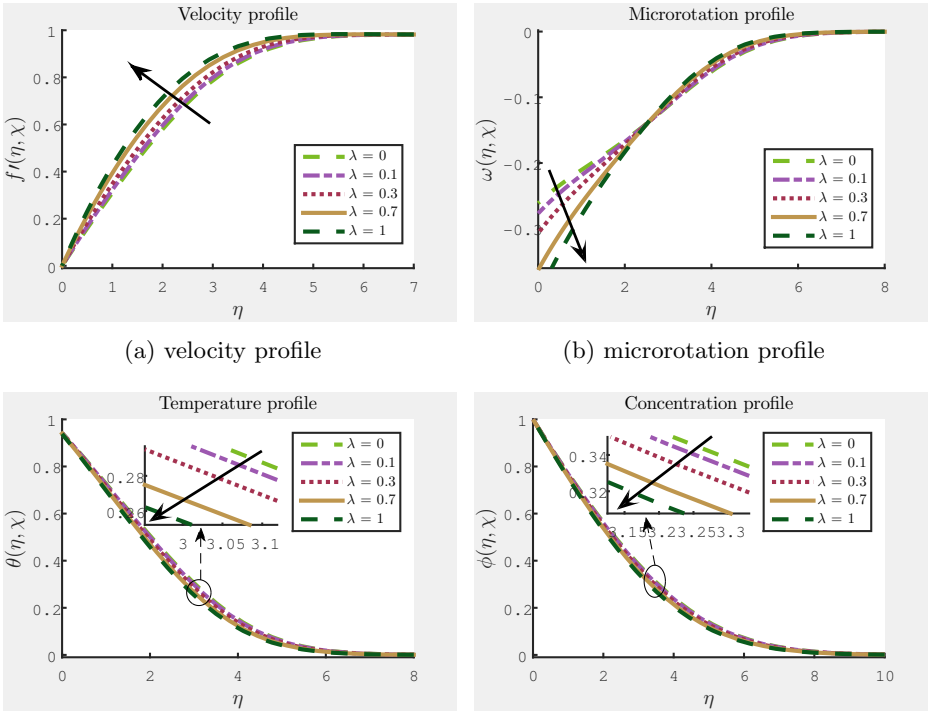

(a) velocity profile (b) microrotation profile

(c) temperature profile (d) concentration profile

FIGURE 8. Effect of mixed convection λ on the flow profiles

Acknowledgement. The authors would like to thank the anonymous reviewers for the valuable comments that improved the quality of the study.

References

1. D. B. Ingham, *Transport phenomena in porous media*, Pergamon Press, Oxford, 1998.
2. D. A. Nield, A. Bejan, *Convection in porous media, third ed.*, Springer-Verlag, New York, 2006.
3. H. C. Chien, K. C. Chao, *Non-Darkin mixed convection along a vertical plate embedded in a porous medium*, Appl. Math. Modelling **14** (1990), 482–488.
4. S. R. Sheri, M. D. Shamshuddin, *Diffussion-thermo and chemical reaction effects on an unsteady MHD free Convection flow in a micropolar fluid*, Theor. Appl. Mech. **43** (2016), 117–131.
5. T. Y. Na, J. P. Chiou, *Laminar natural convection over a frustum of a cone*, Appl. Sci. Res. **35** (1979), 409–421.
6. S. G. Mohiddin, O. A. Beg, S. V. K. Varma, *Numerical study of free convective MHD flow past a vertical cone in non-Darcian porous media*, Theor. Appl. Mech. **41** (2014), 119–140.
7. C. Y. Cheng, *Natural convection of a micropolar fluid from a vertical truncated cone with power-law variation in temperature*, Int. Commun. Heat Mass Transf. **35** (2008), 39–46.
8. F. N. Lin, *Laminar free convection from a vertical cone with uniform surface heat flux*, Letters in Heat and Mass Transfer **3** (1976), 49–58.

9. K. Vajravelu, L. Nayfeh, *Hydromagnetic convection at a cone and a wedge*, Int. Commun. Heat. Mass. Transf. **19** (1992), 701–710.
10. K. A. Yih, *Effect of radiation on natural convection about a truncated cone*, Int. J. Heat Mass Transfer **42** (1999), 4299–4305.
11. A. J. Chamkha, A. R. A. Khalid, O. Al-Hawaj, *Simultaneous heat and mass transfer by natural convection from a cone and a wedge in porous media*, J. Porous Media **3** (2000), 155–164.
12. B. Pullepu, K. Ekambavanan, A. J. Chamkha, *Unsteady laminar free convection from a vertical cone with uniform surface heat flux*, Nonlinear Anal., Model. Control **13** (2008), 47–60.
13. M. S. Gouse, V. R. Prasad, S. V. K. Varma, B. O. Anwar, *Numerical study of unsteady free convective heat and mass transfer in a walters-B viscoelastic flow along a vertical cone*, Int. J. Appl. Math. Mech. **6** (2010), 88–114.
14. A. Postelnicu, *Free convection from a truncated cone subject to constant wall heat flux in a micropolar fluid*, Meccanica **47** (2012), 1349–1357.
15. A. Postelnicu, *Free convection about a vertical frustum of a cone in a micropolar fluid*, Int. J. Eng. Sci. **44** (2006), 672–682.
16. A. J. Chamkha, S. Abbasbandy, A. M. Rashad, K. Vajravelu, *Radiation effects on mixed convection about a cone embedded in a porous medium filled with a nanofluid*, Meccanica **48** (2013), 275–285.
17. , F. O. Patrulescu, T. Groan, I. Pop, *Mixed convection boundary layer flow from a vertical truncated cone in a nano fluid*, Int. J. Numer. Method. H. **24** (2014), 1175–1190.
18. A. C. Eringen, *Simple microfluids*, Int. J. Eng. Sci. **2** (1964), 205–217.
19. A. C. Eringen, *Theory of micropolar fluids*, J. Math. Mech. **16** (1966), 1–18.
20. T. Ariman, M. A. Turk, N. D. Sylvester, *Microcontinuum fluid mechanics-a review*, Int. J. Eng. Sci. **11** (1973), 905–930.
21. T. Ariman, M. A. Turk, N. D. Sylvester, *Applications of microcontinuum fluid mechanics*, Int. J. Eng. Sci. **12** (1974), 273–293.
22. G. Lukaszewicz, *Micropolar fluids-Theory and Applications*, Birkhauser, Springer Science & Business Media, Basel, 1999.
23. S. S. Motsa, I. L. Animasaun, *Paired Quasi-Linearisation analysis of heat transfer in unsteady mixed convection Nanofluid containing both nanoparticles and gyrotactic microorganisms due to impulsive motion*, J. Heat Transf. **138** (2016), 114503–114511.
24. R. E. Bellman, R. E. Kalaba, *Quasilinearization and nonlinear boundary-value problems*, Rand corporation, New York, 1965.
25. L. N. Trefethen, *Spectral methods in MATLAB*, SIAM, Philadelphia, 2000.
26. S. S. Motsa, I. L. Animasaun, *Paired Quasi-Linearisation analysis of heat transfer in unsteady mixed convection Nanofluid containing both nanoparticles and gyrotactic microorganisms due to impulsive motion*, J. Heat Transf. **138** (2016), 114503–114511.
27. O. Otegbeye, S. S. Motsa, *A paired quasilinearization method for solving boundary layer flow problems*, AIP Publishing, 2018, 030020–030029.

МЕТОДА УПАРЕНЕ КВАЗИЛИНЕАРИЗАЦИЈЕ ЗА РЕШЕЊАВАЊЕ МХД МЕШОВИТОГ КОНВЕКЦИЈСКОГ ТОКА МИКРОПОЛАРНОГ ФЛУИДА КРОЗ ЗАРУБЉЕНИ КОНУС У НЕ-ДАРСИЈЕВОЈ ПОРОЗНОЈ СРЕДИНИ

Резиме. Циљ овог рада је да се испита ток, пренос топлоте и масе микрополарног флуида кроз зарубљени конус у не-Дарсијевој порозној средини у присуству попречног магнетног поља разматрањем хемијских реакција и ефеката зрачења. Нелинеарне једначине тока решавају се помоћу методе упарене квазилинеаризације (PQLM). Студија открива да пораст параметра зрачења, мешани конвекцијски параметар и Forchheimer-ов број смањује микроротацију. Такође се примећује да повећање параметра зрачења доводи до одговарајућег повећања и брзине и температуре флуида.

Department of Mathematics
University of Swaziland
Swaziland
mekk_aya@yahoo.com

Department of Mathematics
University of Swaziland
Swaziland
sandilemotsa@gmail.com

Department of Mathematics
University of KwaZulu-Natal
South Africa
muyiwabowen@yahoo.com

(Received 10.08.2019.)
(Revised 22.11.2019.)
(Available online 24.12.2019.)